

Electronic Supplementary Information (ESI)

H₂O₂/steam activation as an eco-friendly and efficient top-down approach to enhancing porosity on carbonaceous materials: the effect of inevitable oxygen functionalities on CO₂ capture

Young-Jung Heo and Soo-Jin Park*

Department of Chemistry, Inha University, 100 Inharo, Incheon 22212, Korea

* Corresponding authors. Tel.: +82-32-876-7234; Fax: +82-32-867-5604.

E-mail address: sjpark@inha.ac.kr (S. -J. Park)

Calculation of Henry's law selectivity and isosteric heat of adsorption (ΔH_{ads})

To obtain reliable Henry's constants, a virial-type¹ expression comprising the temperature-independent parameters a_i and b_i was applied;

$$\ln P = \ln N + \frac{1}{T} \sum_{i=0}^m a_i N^i + \sum_{i=0}^n b_i N^i$$

Where P , N , and T are the pressure, adsorbed amount, and temperature, respectively. a_i and b_i are virial coefficients, which are the temperature independent fitting parameters. m and n represent the number of coefficients required to adequately describe the isotherms. The fitting of all isotherms in this work have R^2 greater than 0.999. The Henry's constant (K) at the temperature T can be calculated;

$$K = \exp(-b_0) \cdot \exp(-a_0/T)$$

The Henry's law selectivity for pure gas component i over j is given as;

$$S_{ij} = K_i / K_j$$

The Henry's constants and fitting parameters for SAC, HAC20, and R-HAC20 are listed in Table S2. The isosteric heat of adsorption (ΔH_{ads}) was calculated using the adsorption data collected at 273 K, 298 K, and 313 K and the Clausius-Clapeyron equation.

$$\Delta H_{ads} = -R \left[\frac{d \ln P}{d(1/T)} \right]$$

where R is the gas constant, and P is the equilibrium partial pressures of CO₂ adsorbed at given temperature T.

Ideal Adsorption Solution Theory (IAST) method

The ideal adsorbed solution theory (IAST) developed by Myers and Praunitz for predict binary mixture adsorption from the experimental pure gas isotherms.² In order to perform the IAST calculations, the single component isotherms should be fitted by a proper model. The single-site Langmuir-Freundlich (SSLF) and dual-site Langmuir-Freundlich (DSLF) models were adopted to correlate the pure-component equilibrium data and predict the adsorption of mixture.^{3,4} The SSLF and DSLF models can be defined as,

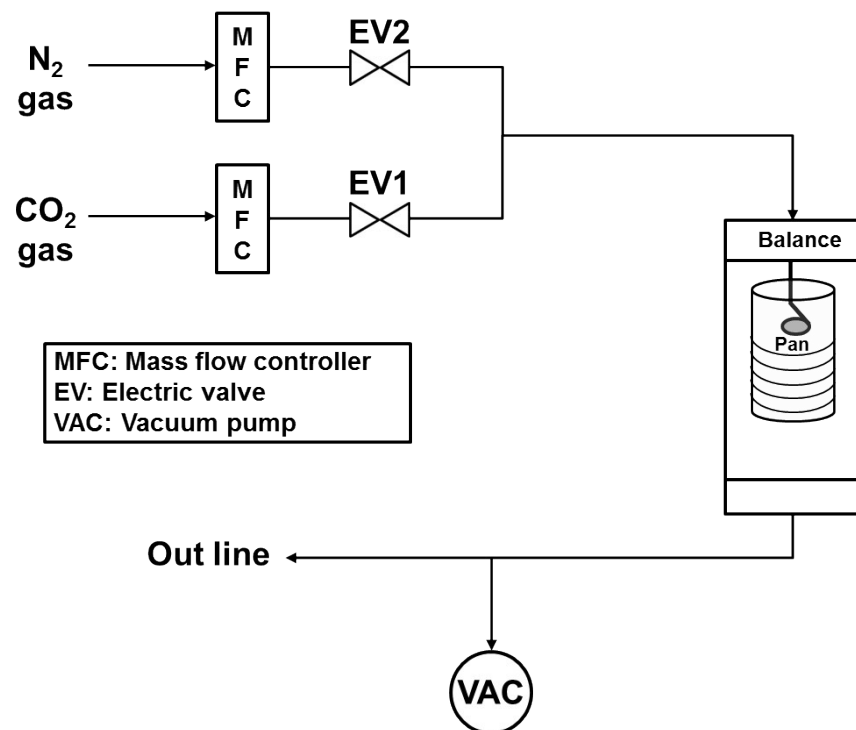
$$SSLF : q = \frac{q_{sat} b P^n}{1 + b P^n}$$

$$DSLF : q = q_A + q_B = \frac{q_{sat,A} b_A P^{n_A}}{1 + b_A P^{n_A}} + \frac{q_{sat,B} b_B P^{n_B}}{1 + b_B P^{n_B}}$$

where, q is molar loading of adsorbate, q_{sat} is saturation loading, b is parameter in the pure component Langmuir-Freundlich adsorption isotherm, A and B are referring to two different sites. To investigate the separation of binary mixtures, the adsorption selectivity can be defined as,

$$S_{i/j} = \frac{x_i / y_i}{x_j / y_j}$$

Where the selectivity refers to the first component over the second one, the x_i , x_j denote the molar fractions of species i, j in the adsorbed phase, and y_i , y_j denote the molar fractions of species i, j in the bulk phase.



Scheme S1 Experimental setup of the binary mixture gas adsorption (gravimetric analysis) and cycling measurements.

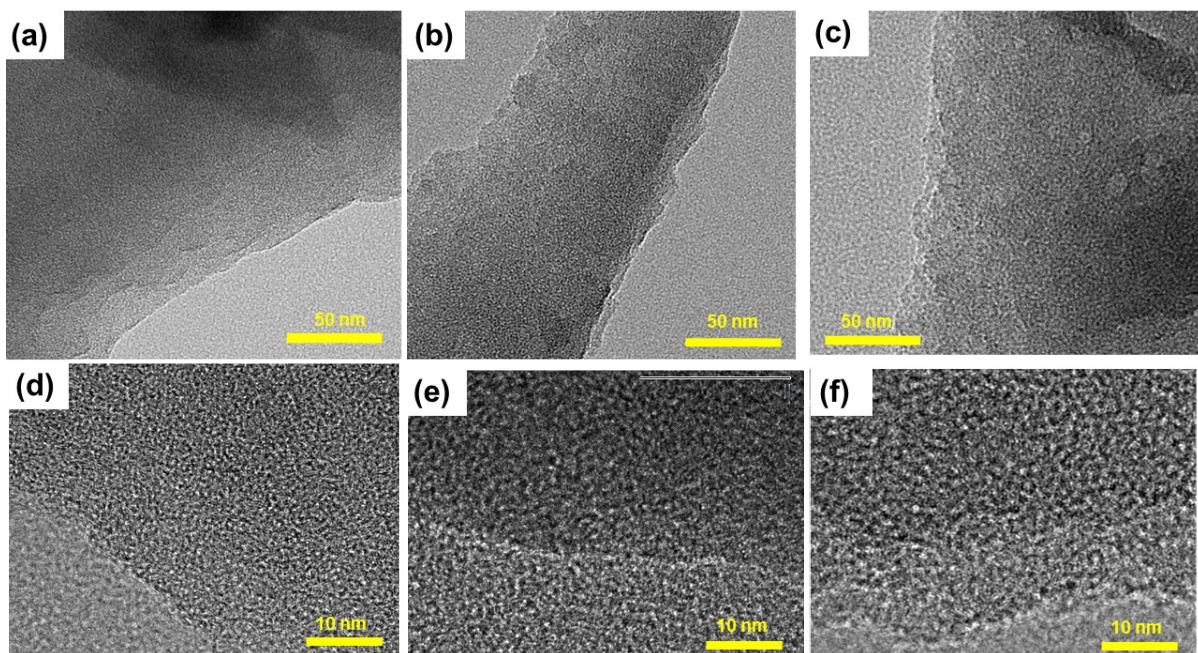


Fig. S1 FE-TEM images of the (a,d) SAC, (b,e) HAC20, and (c,f) R-HAC20, respectively.

Table S1 Comparison between the chemical composition obtained by elemental analysis and XPS.

Specimens	Elemental analysis (wt.%)			XPS (wt.%)		
	C	H	O	C	H	O
MC	86.01	2.67	11.32	84.90	3.04	12.06
SAC	93.62	0.87	5.51	92.18	1.19	6.63
HAC20	92.43	1.01	6.56	88.56	1.81	9.63
R-HAC20	94.27	0.62	5.11	93.83	0.86	5.31

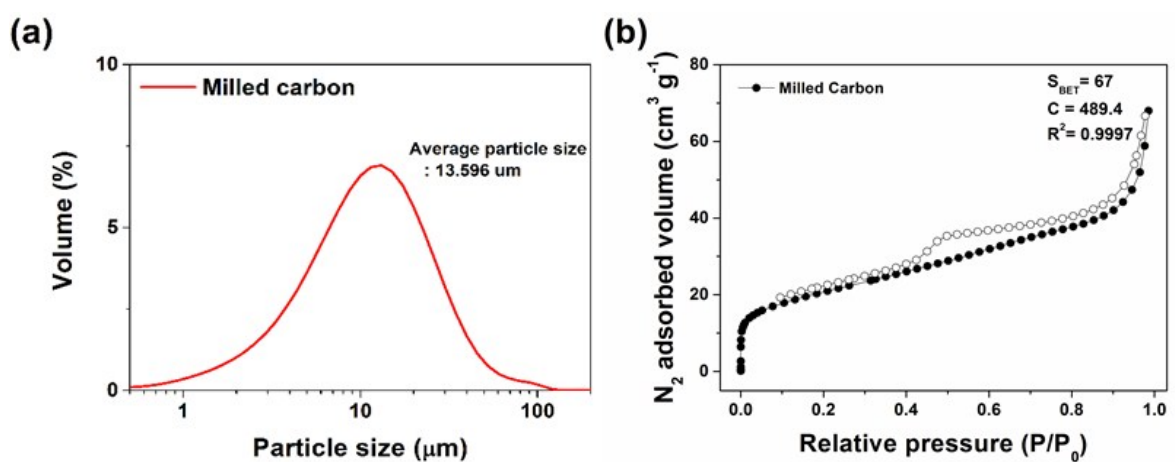


Fig. S2 (a) Particle size distribution and (b) 77K/ N_2 isotherms of Milled carbon.

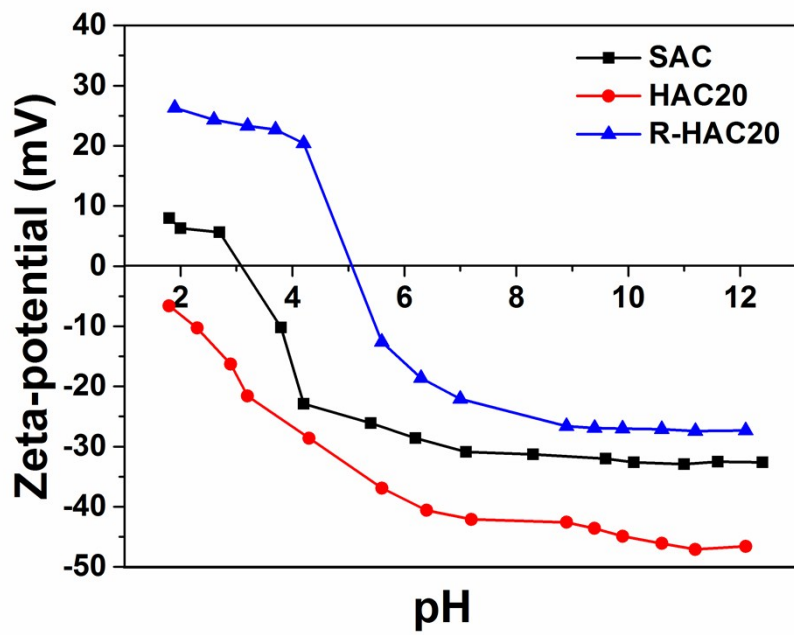


Fig. S3 pH dependent zeta-potential curves of the SAC, HAC20, and R-HAC20.

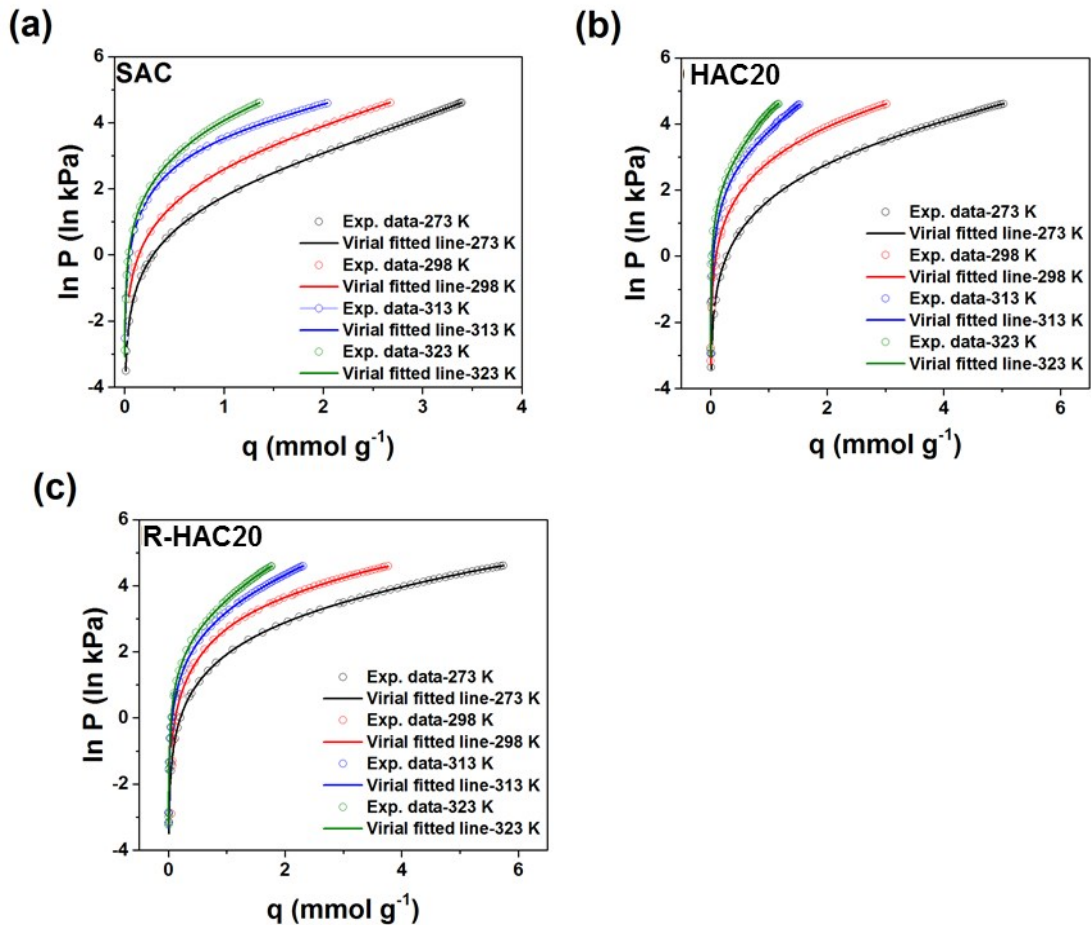


Fig. S4 Virial fitting results for CO_2 adsorption of the samples at various temperatures.

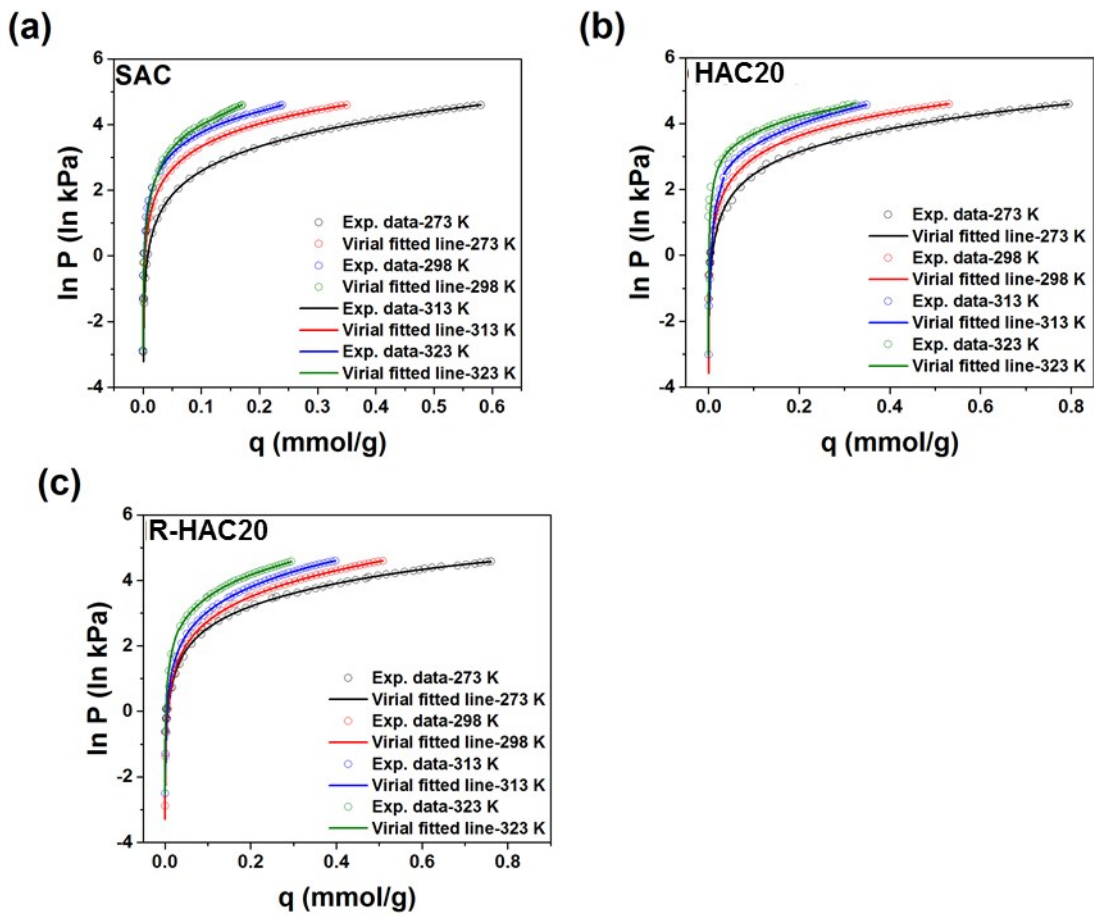


Fig. S5 Virial fitting results for N_2 adsorption of the samples at various temperatures.

Table S2 Henry's constant (K) and virial fitting results for SAC, HAC20 and R-HAC20.

Specimens		K_{CO_2} (mmol g ⁻¹ kPa ⁻¹)	K_{N_2} (mmol g ⁻¹ kPa ⁻¹)	CO ₂ fitting R^2	N ₂ fitting R^2
SAC	273 K	0.36578	0.00680	>0.9999	0.9999
	298 K	0.16335	0.00489	>0.9999	0.9997
	313 K	0.07334	0.00255	0.9999	0.9996
	323 K	0.04609	0.00217	>0.9999	0.9998
HAC20	273 K	0.33706	0.00853	>0.9999	0.9999
	298 K	0.15184	0.00504	0.9999	0.9998
	313 K	0.05494	0.00226	0.9996	0.9999
	323 K	0.03241	0.00201	0.9998	0.9993
R-HAC20	273 K	0.22614	0.00712	>0.9999	0.9999
	298 K	0.13833	0.00493	>0.9999	0.9996
	313 K	0.05202	0.00191	0.9998	0.9997
	323 K	0.04868	0.00188	0.99999	0.9998

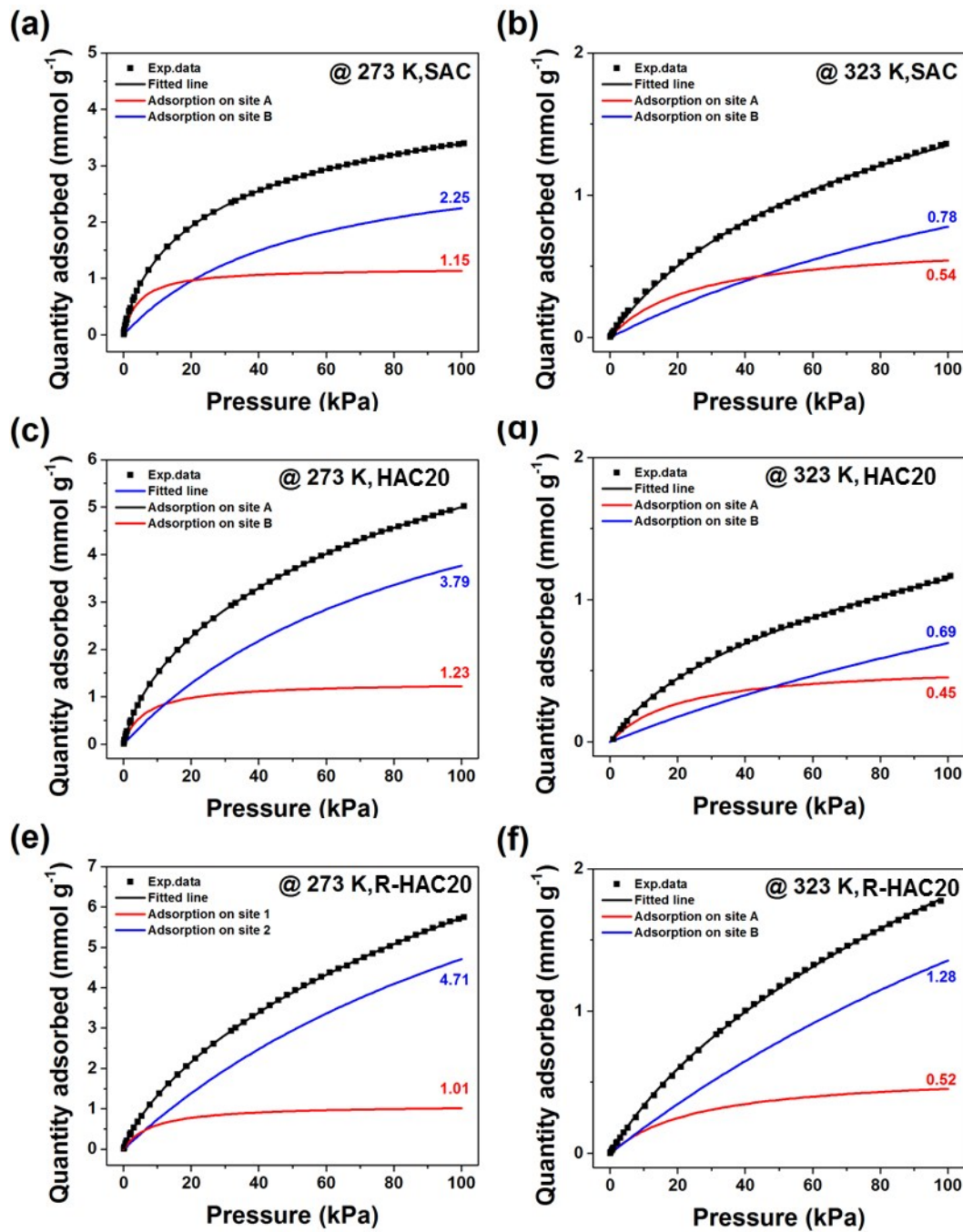


Fig. S6 Dual-site Langmuir-Freundlich fitting results for CO₂ adsorption of the samples at 273 K and 323 K. Plots are experimental results. Black, red and blue lines show DSLF model correlation, adsorption on site 1, and adsorption site on 2, respectively. The detailed fitting parameters are presented in the Table S3.

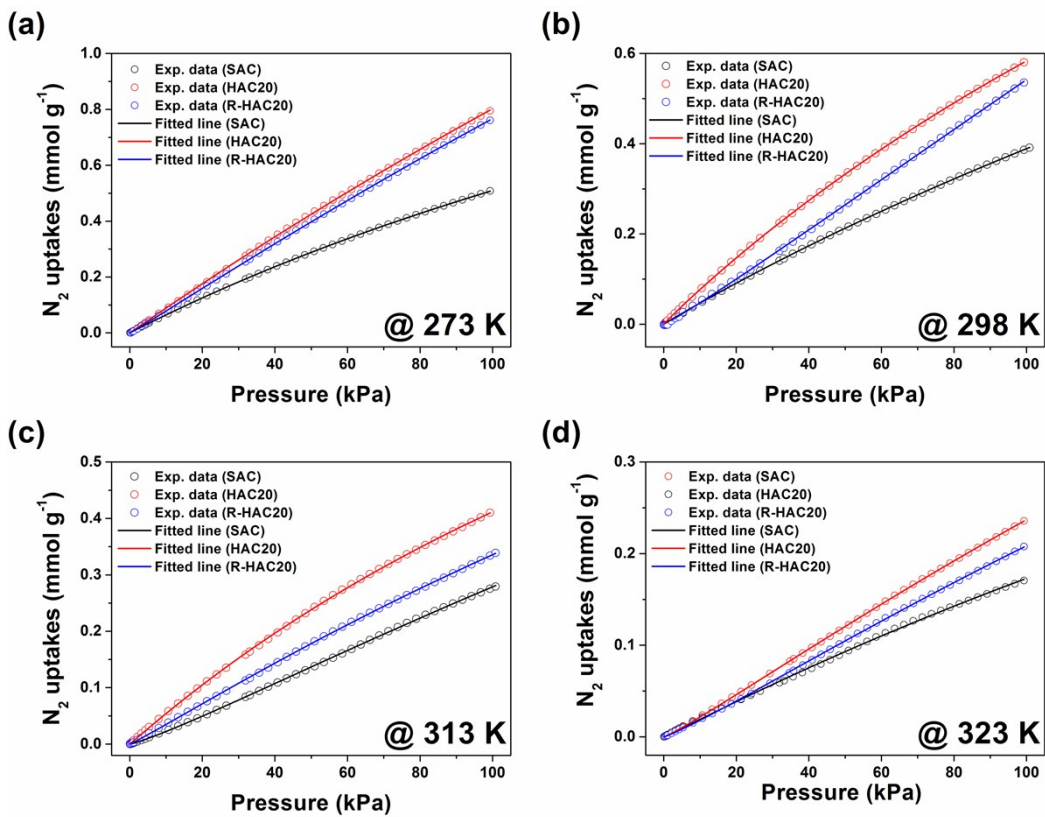


Fig. S7 Single-site Langmuir-Freundlich fitting results for N_2 adsorption of the samples at various temperatures. The detailed fitting parameters are presented in the Table S4.

Table S3 Dual-site Langmuir-Freundlich fitting parameters of CO₂ adsorption.

Specimens		$q_{sat,A}$ (mmol g ⁻¹)	$q_{sat,B}$ (mmol g ⁻¹)	b_A (kPa ⁻¹)	b_B (kPa ⁻¹)	n_A	n_B	R^2
SAC	273 K	1.18706	3.40177	0.21902	0.01945	1.00450	0.99954	0.9999
	298 K	1.03009	3.22035	0.10295	0.01102	1.02980	0.98975	0.9998
	313 K	0.89003	2.55921	0.08747	0.00872	1.00186	0.99961	0.9999
	323 K	0.68538	2.35577	0.04097	0.00512	1.01872	0.99765	0.9998
HAC20	273 K	1.32062	7.47576	0.17002	0.01076	1.06219	1.01245	0.9999
	298 K	0.99358	5.52628	0.09407	0.00713	1.00995	0.99891	0.9999
	313 K	0.68073	3.05535	0.05458	0.00464	1.01849	0.99524	0.9991
	323 K	0.54202	2.70426	0.04604	0.00354	0.97603	1.00526	0.9996
R-HAC20	273 K	1.09880	11.76727	0.11941	0.00666	1.00192	0.99991	0.9999
	298 K	0.75199	9.63336	0.05041	0.00484	0.97059	1.00238	0.9997
	313 K	0.58832	7.14505	0.04315	0.00425	0.98865	1.00053	0.9998
	323 K	0.57105	4.98258	0.03819	0.00373	0.99745	0.99936	0.9999

Table S4 Single-site Langmuir-Fruendlich fitting parameters of N₂ adsorption.

Specimens		q_{sat} (mmol g ⁻¹)	b (kPa ⁻¹)	n	R^2
SAC	273 K	3.77866	0.00207	1.06344	0.9999
	298 K	2.60898	0.00191	1.01941	0.9999
	313 K	2.11240	0.00146	0.99942	0.9994
	323 K	1.76452	0.00118	1.01654	0.9995
HAC20	273 K	4.69484	0.00214	1.01347	0.9991
	298 K	4.45483	0.00208	1.07169	0.9998
	313 K	3.47217	0.00174	1.05436	0.9989
	323 K	1.36747	0.00146	0.92984	0.9996
R-HAC20	273 K	4.50774	0.00164	0.95669	0.9991
	298 K	3.23737	0.00149	0.94289	0.9993
	313 K	2.46076	0.00137	0.96184	0.9998
	323 K	1.56532	0.00112	0.93773	0.9994

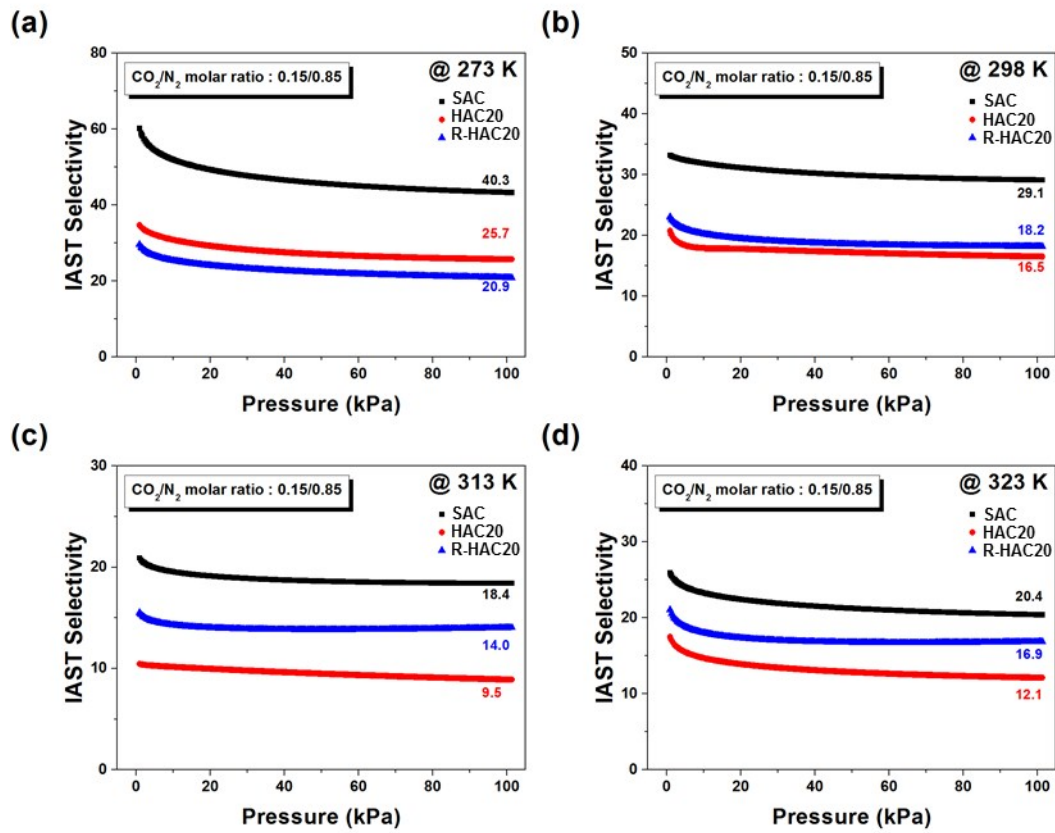


Fig. S8 IAST-predicted adsorption selectivities of CO_2/N_2 using 0.15/0.85 CO_2/N_2 molar ratio at various temperatures.

Table S5 CO₂ capturing performances of (i.e. CO₂ uptakes, adsorption rates and CO₂ uptake retention) of the samples evaluated under flue gas condition (15% CO₂ /85% N₂) at various temperatures.

Specimens		293 K	303 K	313 K	323 K
SAC	CO ₂ uptakes ^a (mg g ⁻¹)	33.5	28.5	21.7	17.7
	Adsorption rates ^b (mg g ⁻¹ min ⁻¹)	8.0	7.7	7.2	6.2
	CO ₂ uptake retention ^c (%)	100	85.1	64.8	52.8
HAC20	CO ₂ uptakes (mg g ⁻¹)	41.2	28.6	21.2	11.1
	Adsorption rates (mg g ⁻¹ min ⁻¹)	9.4	7.3	2.7	0.4
	CO ₂ uptake retention (%)	100	69.4	51.5	26.9
R-HAC20	CO ₂ uptakes (mg g ⁻¹)	58.9	39.4	33.3	28.5
	Adsorption rates (mg g ⁻¹ min ⁻¹)	32.1	25.1	15.0	7.1
	CO ₂ uptake retention (%)	100	66.9	56.5	48.4

^a CO₂ uptakes were investigated for 60 min under flue gas condition at various temperatures.

^b Adsorption rates were determined from the highest value of the first derivation of CO₂ adsorption curves.

^c CO₂ uptake retentions over the temperature rage with respect to the uptakes at 293 K using gravimetric method.

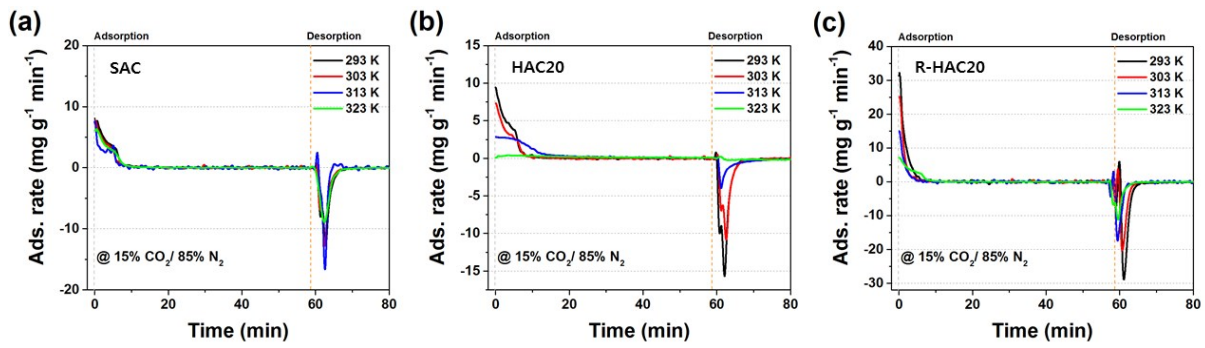


Fig. S9 Time-dependent CO₂ adsorption rates of the samples evaluated under flue gas condition (15% CO₂ /85% N₂) at various temperatures. These results were obtained from the first derivation of the obtained adsorption curves at various temperatures.

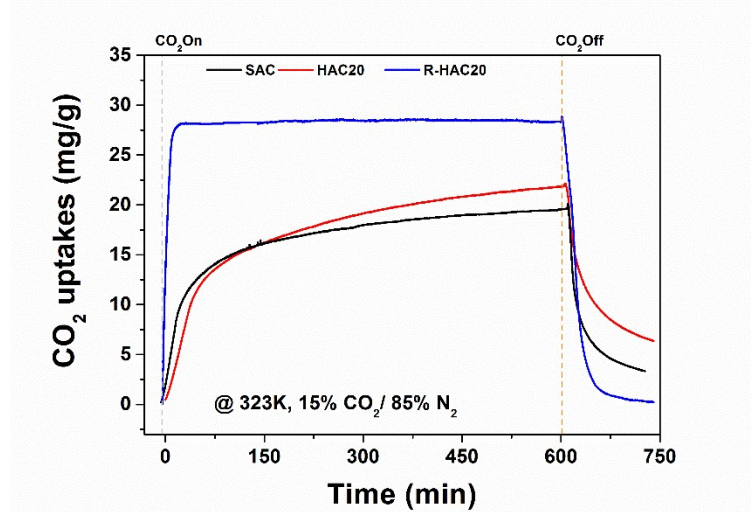


Fig. S10 Time-dependent CO₂ adsorption–desorption curves of the samples for 10 h, respectively.

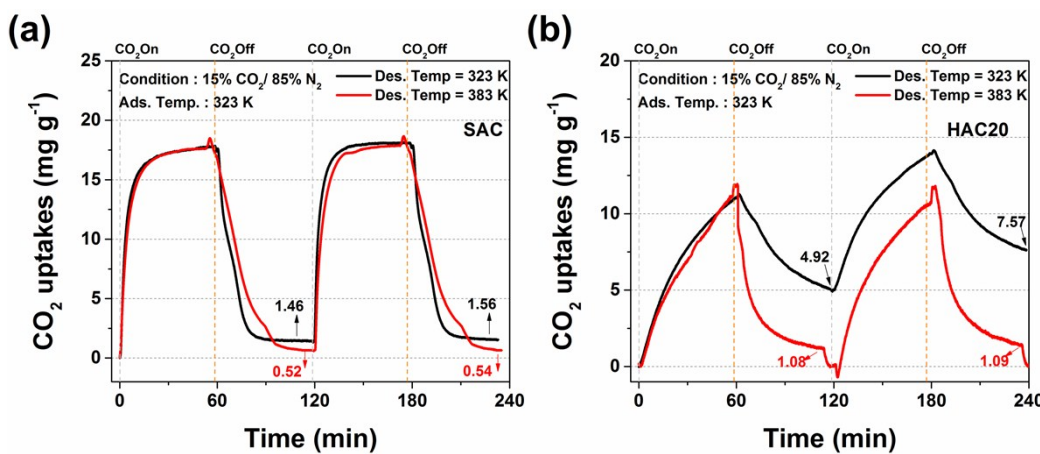


Fig.S11 Time-dependent CO_2 adsorption–desorption curves of the (a) SAC and (b) HAC20 over different desorption cycles for regeneration.

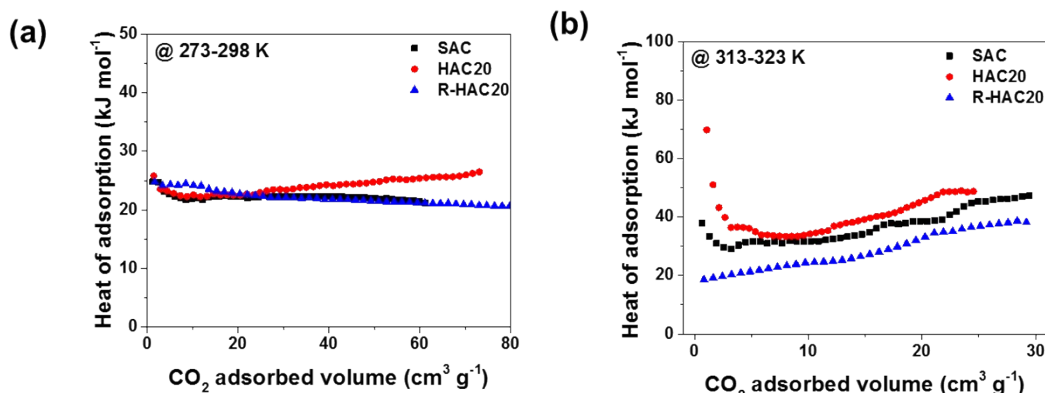


Fig. S12 Isosteric heat of adsorption of the samples using a Clausius–Clapeyron equation, obtained from CO_2 isotherms at low (273–298 K) and high (313–323 K) temperature ranges, respectively.

References

- 1 L. Czepirski, J. JagieŁŁo, *Chem. Eng. Sci.* 1989, **44**, 797-801.
- 2 A. Myers, J. M. Prausnitz, *AIChE J.* 1965, **11**, 121-127.
- 3 T. Islamoglu, S. Behera, Z. Kahveci, T. Tessema, P. Jena, H. M. El-Kaderi, *ACS Appl. Mater. Interfaces* 2016, **8**, 14648-14655.
- 4 Y. Bae, O. K. Farha, J. T. Hupp, R. Q. Snurr, *J. Mater. Chem.* 2009, **19**, 2131-2134.